Studying ionizing shock wave by IR diagnostic techniques

R. I. SOLOUKHIN, YU. A. YACOBI and V. I. YACOVLEV (NOVOSIBIRSK)

MEASUREMENTS were made of the electron concentration profiles behind strong shock waves propagating in argon at shock Mach numbers between 10 and 13. A complex multipurpose CO_2-laser-interferometer technique was developed to study the time histories of the electron densities as also the plasma absorption coefficients and electron temperatures across the shock wave. Electron temperatures and ionization rate constants were evaluated.

Wykonano pomiary profilów koncentracji elektronów za silnymi falami uderzeniowymi roz-przestrzeniającymi się w argonie przy liczbach Macha od 10 do 13. Rozwinięto skomplikowaną, wielozadaniową technikę pomiarową laserowo-interferometryczną dla analizy przebiegu zmian czasowych koncentracji elektronów jak również dla pomiaru współczynników absorbcji plazmy i temperatury w przekroju poprzecznym fali uderzeniowej. Obliczono temperaturę elektronów i współczynniki prędkości jonizacji.

Произведены измерения профилей концентрации электронов за сильными ударными волнами, распространяющимися в аргоне при числах Маха от 10 до 13. Разработана комплексная, универсальная измерительная лазерно-интерферометрическая техника для анализа процесса временных изменений концентрации электронов, а также для измерения коэффициентов абсорбции плазмы и температуры в поперечном сечении ударной волны. Оценены температура электронов и коэффициенты скорости ионизации.

Introduction and basis of the method

THOUGH many aspects of the ionization kinetics behind the shock front of noble gases has been studied extensively [1, 2], some essential details of the ionization reaction mechanisms are still not understood clearly and the problem appears to be of a permanent interest for basic developments of shock ionization kinetics and their applications in high-temperature gasdynamics. The purposes of this investigation were to determine in greater detail the variation of electron densities, and to evaluate the electron temperatures in a shocked gas using novel IR-diagnostic techniques which make it possible to follow the transient electron concentration and plasma absorption coefficients behind an ionizing shock front with high detection sensitivities and perfect time resolutions.

The most applicable optical methods developed to study the ionized gas states can be separated into two large groups: (a) measuring techniques which are based on the refractive index variations, such as schlieren or interferometer methods; and (b) gas emission and absorption measurements which are based, under equilibrium conditions, on the validity of Kirchhoff's law. The informative uses of these methods depend essentially on the light wavelength value λ. The plasma refractive index for monochromatic light can be written as

$$(1) \qquad n-1 = -AN_e\lambda^2+BN_0,$$

where N_e and N_0 are the electron and atom number densities, respectively, $A = 4.46 \cdot 10^{-14}$ cm [3]. In the infrared spectral region, the first term in the Eq. (1) is of a

few orders of value higher than the second; therefore, any phase changes in a probing light beam introduced by a plasma under test are completely determined by the charged particles component only, and the relative sensitivity of the method to the electron density determination is increased as a square of the wavelength. Thus the electron concentration of a partially ionized gas is simply determined from a phase change $\Delta\varphi$ using an appropriate interferometer technique in measurements:

$$(2) \qquad \Delta\varphi = 2\pi A N_e L \lambda,$$

where L is an optical path of a probing beam in a plasma. Information of this kind can be essentially supplemented by measurements of the plasma density gradients ∇N_e by means of a schlieren method:

$$(3) \qquad \beta = -A\lambda^2 L \nabla N_e,$$

where β is an angle of the parallel beam inclination in a non-uniform plasma. Finally, the measurements of light absorption coefficients K, in a continuum spectrum including the stimulated emission, may also serve as a source of information on plasma densities and temperatures since

$$(4) \qquad K = C(T)\lambda^2 N_e^2.$$

It is seen that the plasma temperature can be extracted using the Eq. (4) if the electron concentration N_e is determined independently by way of (2) and (3). Since in all these techniques, only non-dimensional variable parameters are determined, rather high detection sensitivities can be achieved. The lower limit of a method of application can be determined from a minimum detectable deviation of the initial value, δ, in the experiment. For instance, in the interferometer measurements

$$(5) \qquad (N_e)_{\min}^i \approx \frac{\delta_i}{A\lambda L}.$$

The following assumptions can be made in evaluations of the schlieren method sensitivities, (a) the focused laser beam diameter d is determined by a diffraction divergence d_0/λ, where d_0 is the initial beam diameter, and (b) a characteristic size of an electron density gradient in a relaxation zone is of the order of the shock tube diameter. Then

$$(6) \qquad (N_e)_{\min}^s \approx \frac{\delta_s}{A\lambda d_0}.$$

In order to evaluate the detection sensitivity of an absorption technique [4], it is necessary to take into account that (a) $1, = k78 \cdot 10^{-2} g_{ff} \nu^{-2} T_e^{-3/2} N_e^2$, where g_{ff} is the Gaunt's factor, and (b) the plasma transparency which can be determined through a beam transmission $\theta = \exp(-KL)$ is recorded in the experiments:

$$(7) \qquad (N_e)_{\min}^a \approx \frac{2 \cdot 10^{11} T^{3/4} [\log(1-\delta_a)]^{1/2}}{L^{1/2}\lambda}.$$

Consider a numerical example assuming $L = 10$cm, $g_{ff} \approx 1$, $d_0 = 0.5$cm, $T = 10^4\,°$K, $\delta_{i,s,a} \sim 0.05$. Then, from (5), (6) and (7), we obtain respectively:

$$(8) \qquad (N_e)_{\min}^i \approx \frac{10^{11}}{\lambda}, \qquad (N_e)_{\min}^s \approx \frac{2 \cdot 10^{12}}{\lambda}, \qquad (N_e)_{\min}^a \approx \frac{2 \cdot 10^{13}}{\lambda},$$

where λ is in cm.

The maximum electron concentrations available to be measured using an active optical diagnostic technique are limited and can be determined by way of the plasma frequency as

$$(N_e)_{max} = \frac{\pi m_e}{\lambda^2 e^2} \approx \frac{10^{13}}{\lambda^2}.$$

It is clearly seen from the above consideration that detection sensitivities of all three methods listed are essentially improved with increase in the light source wavelength. Typical plasma conditions appropriate for various diagnostic techniques are shown in Fig. 1. A sequence of the available laser frequencies He—Ne, CO_2 and HCN lasers as well as microwaves of the 0.8 cm wavelength are indicated specifically in the diagram. The widely used microwave diagnostic techniques [5, 6] easily provide electron concentration measurements in a range of 10^9–10^{13} cm^{-3}, where as is seen in Fig. 1, schlieren and absorp-
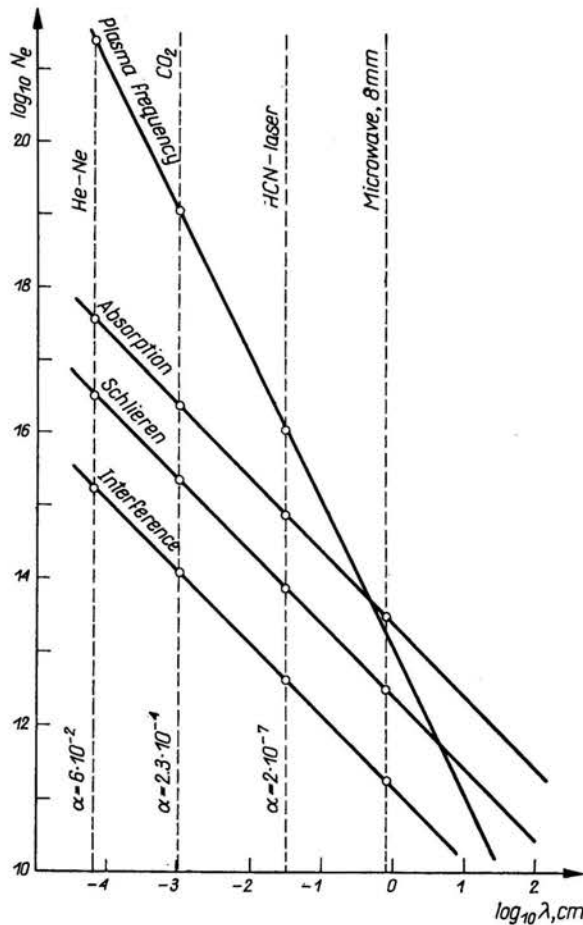
FIG. 1. Diagram illustrating plasma parameter ranges available for applications of various measuring techniques. Minimum plasma densities detectable in the experiments (5 per cent of total value) are plotted as a function of the wavelength of a source of the probing electromagnetic radiation. The plasma frequency limit represents maximum electron number densities detectable using active radiation methods. The dotted lines represent degrees of ionization α required the electron contribution into the plasma refractive index being equal to the effect of neutral atoms.

tion techniques cannot be applied due to the plasma frequency limitation. On the other hand, experimental methods of active diagnostics in the visible measurements of plasma densities in a range between 10^{15} and $10^{21} cm^{-3}$ [3], and it should be taken into account that the degrees of ionization which correspond to equal contributions of the charged and neutral particle contributions into the refractive index of the partially ionized gas, are evaluated to be of the order of 0.1.

The most interesting range of electron concentrations between 10^{13} and $10^{17} cm^{-3}$ appears to be appropriate for infrared diagnostic techniques [7–10], and the degrees of ionization can, under these conditions, be within $\alpha \sim (10^{-1} - 10^{-5})$.

Note that the developments of IR diagnostic techniques have been greatly facilitated during last few years due to applications of molecular lasers, such as CO_2-lasers, used as a light source in various methods of active plasma diagnostics. As illustrated in experiments described below, a complex of various interrelated IR diagnostic techniques appears to be the most effective tool in studies of ionization relaxations in shock waves.

Experimental investigation

The purpose of these experiments was to make careful simultaneous measurements of the nonequilibrium electron concentration profiles and the plasma absorption coefficients behind normal shock waves, and from these data to evaluate electron temperatures and ionization rate constants in argon. The high shock velocities required ($M_1 = 10 - 13$) were obtained by performing the experiment in a double-diaphragm shock tube, 3.4 m long and 3 in. diameter, operated at initial pressures of $3 \cdot - 10$ torr. The driver gas in the first chamber was helium at initial pressures of 140 atm preheated up to $550°K$, argon (0.1 − 0.4) atm being used in the second driver chamber. Shock wave velocities were determined by the signals from two ionization-type gauges mounted in the shock tube wall by using a simple electronic computer. The accuracy of the shock speed measurements was estimated to be less than one per cent.

The experimental setup is shown in Fig. 2. The incident laser beam from a conventional cw CO_2-laser, operated in a single-mode, was split by a germanium plate p_1 into the probing and reference beams which then combined by means of plates $p_2 p_3 p_4$.

Germanium was proved to be the most appropriate material for these plates used as beam-splitters, since in the 10 microns spectral region and at thicknesses of 4 mm, the intensities of the transmitted and reflected beams are approximately equal to each other, and the light absorption is not very significant. To avoid accessory multipass interference effects, an edge angle between planes of a plate was made to be of about 1°.

In a Mach-Zehnder interferometer system, the prism sequence $P_1 P_2 P_4$ and the mirror P_3 can be adjusted to obtain the interference pattern in one direction (i.e. along 1,2), and in the other direction (2′, 2″) the joined beams diverge and no interference occurs. These two divergent beams passed through a test plasma sample can be employed for independent measurements of electron density gradients using a schlieren system (2′) and for recording plasma absorption coefficients (2″), as seen in Fig. 2. Space resolutions of the recording channels were essentially improved using a kind of telescopic system (lenses L_1 and L_3) in order to decrease the incident beam diameter up to 1.5 mm. Two
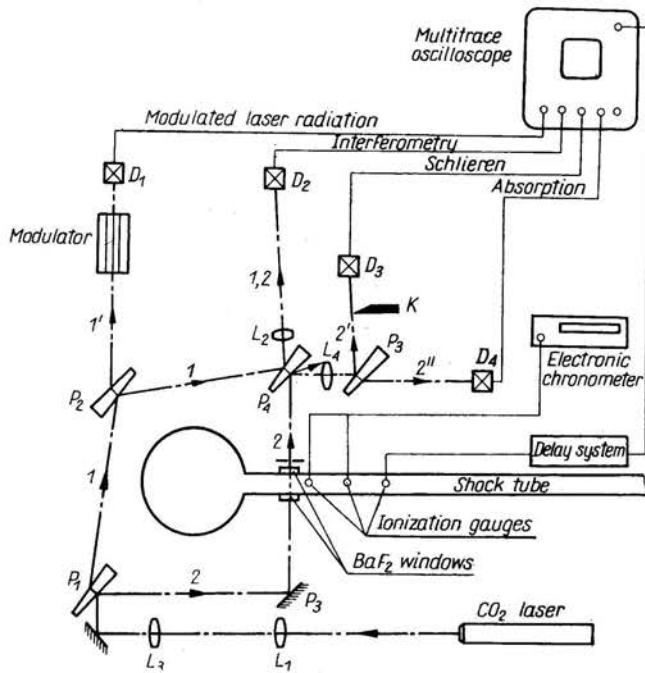
FIG. 2. Experimental setup. Germanium plates (prisms), P, IR lenses, L, and GeAu detectors, D, are noted.

lenses, L_2 and L_4, were located at equal distances of $l = 2f$ (where $f = 25\,\text{cm}$ is the focal length of the lenses) from the subsequent GeAu detectors D_2 and D_4, which were used to detect the interfering (1, 2) and absorbed beam intensities. In addition to the image reproduction functions, these lenses were proved to be extremely helpful in decreasing the laser beam spot displacements at the detector sensing elements caused by strong schlieren effects in a non-uniform plasma sample. In a schlieren system (beam 2′), the knife edge K is located close to the focal point of the lense L_4 and the IR detector D_3 is placed at a short distance from the knife edge. In order to provide the control of the incident laser beam output level, the transmitted beam I' intensity is modulated by a GaAs electro-optical modulating cell and then recorded by a GeAu detector, D_I. The signals from the IR detectors were fed to amplifiers, and then displayed on a multitrace oscilloscope. The rise times of the recording channels were checked to be less than $0.5\ \mu\text{sec}$.

Typical oscilloscope records are shown in Figs. 3 and 4. A moment when the electron concentrations traversed their maximum values behind a shock front is easily detected on these records and corresponds to the rapid changes in rates of the interference fringe shifts which are "counted" in the interferograms to maximum values of the absorption coefficients and to changes in the polarity of the schlieren signals. The maximum magnitude of a schlieren signal corresponds to the maximum rate of the fringe shift. Thus, the general shape of an electron concentration profile is reliably determined by means of simultaneous recording of interference, schlieren and absorption signals. The location of a shock front is clearly detected in the interferogram records as a small-magnitude signal caused by the neutral atom contribution to the refractive index jump, the electron

7*
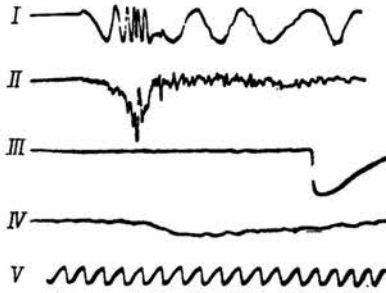
FIG. 3. Typical oscilloscope traces of the interference, schlieren absorption and incident laser radiation signals obtained in one shot simultaneously using a five-trace oscilloscope.
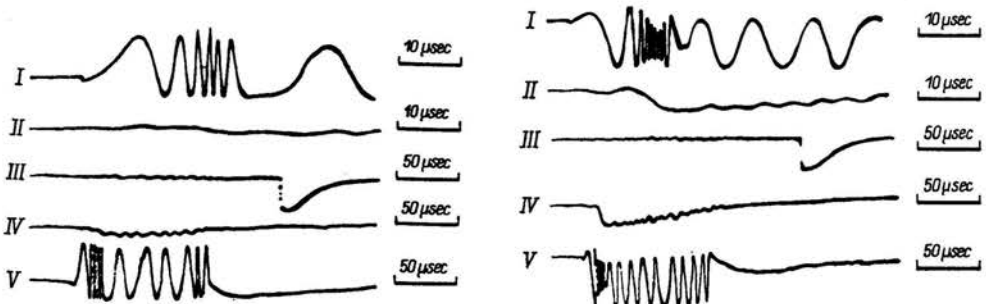
FIG. 4. Typical oscillograms of interference and absorption signals obtained simultaneously in one shot. Two different sweeps are used in this recording.
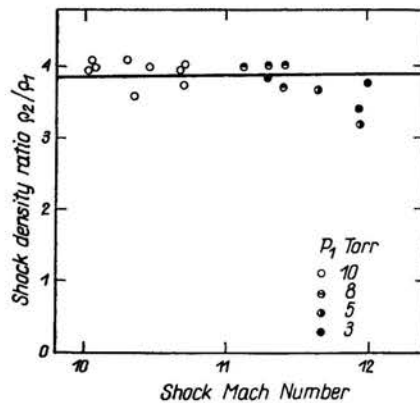
FIG. 5. Measurements of the density ratio behind a shock front in argon.

concentration effects being at this moment negligible. The corresponding phase changes in the interferometer system proved to be quite small: $\Delta\varphi = -(0.02-0.085)\pi$, and were employed to measure the neutral atom density ratios in shock fronts. The results shown in Fig. 5 clearly indicate that the first spike in the interferograms corresponds to the purely neutral component contribution in the shock front density jump. At high shock Mach numbers and low initial pressures, the remarkable deviations from the theoretical gas-dynamic predictions observed may perhaps be explained as a result of effects of the initial

electron concentrations which were evaluated to be of the order of 10^{13} cm^{-3} at $M_1 = 12$ and $p_1 = 3$ torr. Figs. 6 and 7 illustrate typical electron concentration profiles obtained from the interferometer records and represented as a function of the laboratory time. A compari-

FIG. 6. Electron density profiles behind a shock wave in argon. Initial pressure is 3 torr.
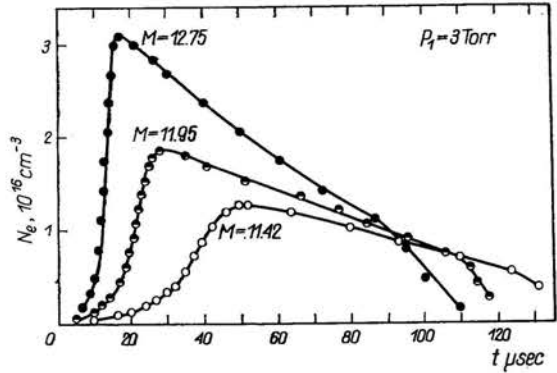
FIG. 7. Electron density profiles behind a shock wave in argon. Initial pressure is 10 torr.
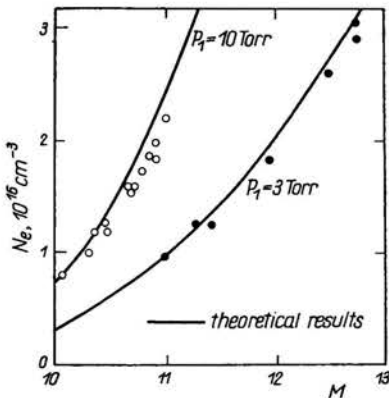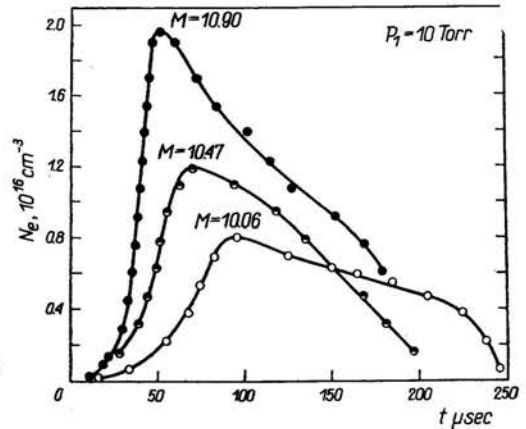
FIG. 8. Comparison between theoretical and experimental maximum electron number densities.
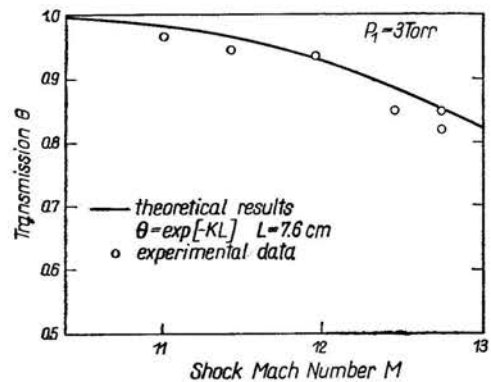
FIG. 9. Comparison between the experimental data on the IR radiation transmission coefficient (at 9.4 micron) with calculation performed for an equilibrium region behind a shock wave in argon.

son between the maximum measured and calculated equilibrium electron concentrations presented in Fig. 8 shows good agreement between these values as well as between predicted and measured magnitudes of the transmitted beam intensities (Fig. 9).

Ionization times are shown in Fig. 10 as a function of the shocked gas temperatures. Note that commercially available argon was used in the experiments; therefore the measured ionization relaxation time experimental points plotted in Fig. 10 are significantly lower than those measured in a low impurity level gas [11, 12] and are close to the experimental
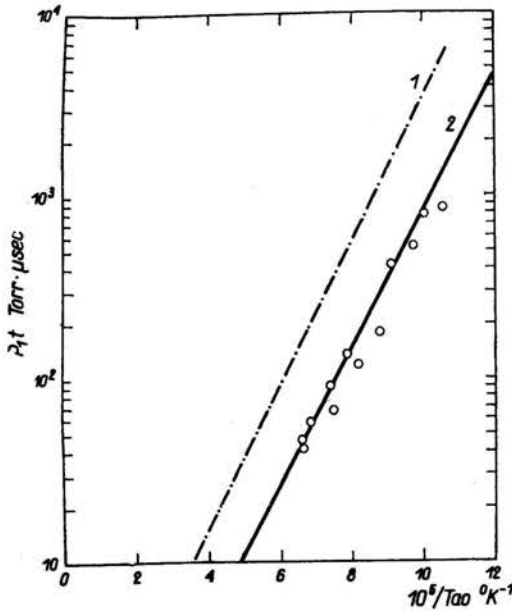
FIG. 10. Ionization relaxation times in argon plotted as a function of $10^5/T_{ao}$, where T_{ao} is the "frozen" temperature behind a shock front.

data obtained in [13, 14]. Figures 6 and 7 show that the electron concentrations behind a shock front are gradually decreased after the maximum value is achieved. The higher shock Mach number the higher the rates of the electron concentration decrease observed, in accordance with the theoretical predictions based on the radiative heat transfer cooling mechanism as assumed in [15, 16].
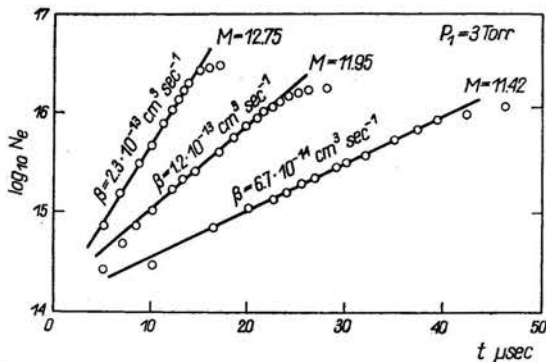
FIG. 11. Electron number density profiles in a relaxation zone behind a shock wave in argon. The electron-atom ionization rate constants β are estimated from the slope of the line.

Initial stages of the electron concentrations rise behind a shock front are presented in Fig. 11 for three shots corresponding to different shock Mach numbers at the same initial pressures of argon. The exponential dependence of N_e on time is observed in a sufficiently wide region of a profile. Such a behaviour of the system can be treated as indicating that the electron impact mechanism is dominant during this stage of the ionization process [2]. Therefore, an effective ionization rate constant β can be derived from the measured electron concentration profiles as follows [15]:

$$(10) \qquad \frac{dN_e}{dt_*} = \beta N_a N_{ev},$$

where t_* is time in the gas particle coordinate system. Generally, β markedly depends on the gas temperature variations within a relaxation zone, but at sufficiently low ionization we may assume approximately

$$(11) \qquad \beta \approx \frac{1}{N_a} \frac{d\log_e N_e}{dt_*}$$

as indicated experimentally (Fig. 11). Since β proved to be approximately constant in the region under consideration, the quasi-steady behaviour of the electron temperature is indicated as shown theoretically in [2, 17, 18]. The dependence of β on electron temperatures in a relaxation zone has been treated in [2] on the basis of diffusion approximation and the real energy structure of an atom. Experimentally, in the case represented in Fig. 11, the effective ionization rate coefficients varied between $6.7 \cdot 10^{-14}$ and $2.3 \cdot 10^{-13}\,\mathrm{cm}^{-3}$. Electron temperatures within time intervals corresponding to the electron-impact-governed stages of the ionization process were estimated from the measured values of β [2] to vary between $12400°K$ and $13600°K$, or slightly higher than the equilibrium gas temperatures behind a shock front.

It should be stressed in conclusion that the combined IR diagnostic techniques based on simultaneous applications of the CO_2-laser interferometry, as also schlieren and absorption measurements are proved to be extremely informative in experimental studies of nonequilibrium transient plasma phenomena. The method is highly reliable and effective in measurements performed in a wide range of plasma densities and temperatures which seem to be the most characteristic for a variety of experiments with low temperature laboratory plasmas.

References

1. E. BAUER, J.Q.S.R.T., 499, 1969; also: M. MERILO, E. I. MORGAN, J. Chem. Phys., **52**, 2192, 1970.
2. D. M. BIBERMAN, A. KH. MNATSAKANIAN, I. T. YAKUBOU [in Russian], Usp. Fiz. Nauk, 102, 431, 1970.
3. R. A. ALPHER, D. R. WHITE, *Optical interferometry*, in "Plasma diagnostic techniques", Acad. Press, New-York-London 1965.
4. I. M. PODGORNY, *Lectures on plasma diagnostics* [in Russian], Atomizdat, 1968.
5. T. I. MC LAREN, R. M. HOBSON, Phys. Fluids, **11**, 2162, 1968.
   also: S. NAKAR, K. KASUYA, C. JAMANACA, Physica, **41**, 213, 1969.
6. G. D. SMECHOV, YU. S. LOBASTOV, J. Techn. Phys., **40**, 1660, 1970.

7. R. I. Soloukhin, Yu. A. Yacobi, Laser and Unconventional Optics Journal, **27**, 3, 1970.

8. R. I. Soloukhin, Yu. A. Yacobi, I.Q.S.R.T., **12**, 25, 1972.

9. R. I. Soloukhin, Yu. A. Yacobi [in Russian], Teplofizika Vysokikh Temperatur, **10**, 1332, 1972.

10. G. D. Petrov, A. I. Petryacov, P. A. Samarskyi [in Russian], Teplofizika Vysokikh Temperatur, **10**, 1, 1972.

11. H. E. Petschek, S. Byron, Ann. Phys., **1**, 20, 1957.

12. B. H. Wong, D. Bershader, J. Fluid Mech., **26**, 459, 1966.

13. G. I. Kozlov, Yu. P. Raizer, D. I. Roitenburg [in Russian], Prikl. Mech. Techn. Phys., **1**, 140, 1968.

14. N. R. Jones, M. Mc Chesney, Nature, 209, 1080, 1966.

15. E. V. Stupochenko, S. A. Losev, A. I. Osipov, *Relaxation processes in shock waves* [in Russian], Nauka, Moscow 1965.

16. G. Kamimoto, K. Teshima, Kyoto University, Rpt. No. CP33, 1972.

17. M. I. Hoffert, H. Lien, Phys. Fluids, **10**, 1769, 1967.

18. G. Kamimoto, K. Teshima, M. Nishimura, Kyoto University, Rpt, No. CP36, 1972.

INSTITUTE FOR PURE AND APPLIED MECHANICS
U.S.S.R. ACADEMY OF SCIENCES, NOVOSIBIRSK.